Structural Study of the Self-Assembled Fullerene Carboxylates: Monoadducts versus Bisadducts

Shuiqin Zhou,* Jianying Ouyang, Patricia Golas, Feng Wang, and Yi Pan

Department of Chemistry of The College of Staten Island, Institute of Macromolecular Assembly, and The Graduate Center, City University of New York, 2800 Victory Boulevard, Staten Island, New York 10314

Received: July 19, 2005; In Final Form: August 18, 2005

Laser light scattering and transmission electronic microscopy have been used to study the self-assembled structures of mono- and bisadducts of fullerene carboxylic acids in tetrahydrofuran (THF) and their sodium salts in aqueous solutions, respectively. In THF, the self-association of monoadducts of fullerene carboxylic acid (MFCA) produces large but narrowly distributed particles with $\langle R_h \rangle \approx 145$ nm. The self-aggregates from the bisadducts of fullerene carboxylic acid (BFCA) in THF are relatively small in size ($\langle R_h \rangle \approx 80$ nm) due to the better solubility. After the ionization of carboxylic acid groups on the C_{60} cage in dilute NaOH solutions, these aggregates dissolved and reorganized. The self-assembly of the monoadducts of sodium carboxylate fullerenes (MSCF) produces small solid spherical particles with $\langle R_h \rangle \approx 32$ nm. The ratio of $\langle R_g \rangle / \langle R_h \rangle \approx 0.83$ indicates that the particles have a nearly uniform density. The increase in concentrations leads to strong interparticle associations to form rodlike and irregularly shaped large aggregates. In contrast, the self-assembly of bisadducts of sodium carboxylate fullerenes (BSCF) results in hollow shells with mainly two different size scales of $\langle R_h \rangle \approx 23$ nm and $\langle R_h \rangle \approx 104$ nm. At high concentrations, the hollow shells associate and melt together to generate three-dimensional networks.

Introduction

Fullerenes and their derivatives have excellent optical and electronic properties as well as special biological activities.[1−8] Moreover, the aggregation state of fullerenes can significantly change the physicochemical properties of fullerenes and thus have a profound influence on the functions of fullerene-based materials.[3,9] However, the low solubility of fullerenes in polar media and the difficulty in controling the aggregation states have represented the main obstacles in the development of nanostructured fullerene materials. With more successful chemical modifications of fullerenes,[10−26] the investigations on the self-assembled structures of amphiphilic fullerene derivatives have attracted increasing research interests recently.[20−27] For example, the self-assembly of C_{60}−*N*,*N*-dimethylpyrrolidinium iodide forms nanorods in dimethyl sulfoxide/water/benzene mixtures and vesicles of various sizes and shapes in water.[20] The self-assembly of potassium salt of pentaphenyl fullerenes produced spherical bilayer nanovesicles in water.[21] Vesicles were found in the aqueous solutions of 1,9-dihydro-bis(11-bromo triammoniumundecanoyloxyl)-1,9-(methanobenzeno methano) fullerenes at concentrations above 3.0 mM.[22] The size of spherical vesicles from the self-assembly of oligo(ethylene glycolated) diphenylaminofluorene in water increases with an increase in concentration.[23] While vesicles are the major morphology observed from the assembly of fullerene derivatives in water, both fibrous- and disklike-aggregated nanostructures were prepared from the self-assembly of C_{60} ammonium amphiphiles.[24]

On the other hand, studies have shown that the morphologies of fullerene aggregates in water could be affected by the molecular structural properties of the hydrophilic side-chain appendage attached on the C_{60} cage. For example, the sizes and morphologies of the self-aggregated C_{60}-end-capped poly(ethylene oxide)s (PEOs) vary with the hydrophilic PEO chain length.[25] The addition of two hydrophilic ethylene oxide units in the spacer between the amino charge and the C_{60} cage of the amino-ethylene fullerenes could induce a sphere-to-rod structural transition. By further attaching a porphyrin macrocycle to the C_{60} cage, nanotubules could be formed.[26,27] Clearly, it is promising to control the self-assembled structures of fullerenes if one can understand how the individual molecular structures of fullerene derivatives determine the self-assembly of fullerenes.

It is expected that the increase in the number of charged appendages on the C_{60} cage could change the water solubility and the hydrophilic/hydrophobic interfacial geometry of the fullerene-based molecules and thus induce different structures of fullerene aggregates. In this work, we compare the structures of self-assembled fullerene aggregates from the monoadducts [C_{60}CH(COOH)] and bisadducts [(HOOC)HCC_{60}CH(COOH)] of fullerene carboxylic acids in THF as well as their corresponding sodium salts in water. Although a cluster formation[28] of the sodium salt of fullerene malonic acid [$C_{60}C(COOH)_2$] and many physical properties[29−31] of sodium salts of fullerene hexamalonic acids [$C_{66}(COOH)_{12}$] in water have been reported, no studies have been carried out to investigate the self-aggregated morphologies of fullerene carboxylates in THF and water. Our findings support that the number of charged appendages on the C_{60} cage is one important structural property of fullerene derivatives to control their self-assembled morphology.

Experimental Section

Materials. C_{60} fullerene (99.9%) was purchased from SES research company, U.S.A. All organic solvents and chemicals of HPLC grade were purchased from Aldrich and used without

* To whom correspondence should be addressed. E-mail: zhoush@mail.csi.cuny.edu.

10.1021/jp053978x CCC: $30.25
Published on Web 09/22/2005

further purification. The water used for sample preparation was purified through a Millipore Milli-Q system with a resistivity of 18.3 MΩ cm. The acidic monoadduct compound 1,2-dihydro-1,2-methanofullerene [60]-61-carboxylic acid [C_{60}CH(COOH)] (**MFCA**) was synthesized, purified, and characterized according to the reported procedures.[32,33] Characterization of C_{60}CH-(COOH): ^{1}H NMR (200 MHz, chloroform-d_1/DMSO-d_6, 1:1): δ 5.09 (s, 1H). FT-IR (KBr): 3435 (m), 2912 (w), 1708 (s), 1427 (s), 1184 (s), 526 (s). ESI-MS: 777 (100, $[M - H]^-$). Bisadducts of fullerene carboxylic acid [(HOOC)HC$_{60}$CH-(COOH)] (**BFCA**) was obtained as follows: The brown fraction, immediately following the monoadducts of (*tert*-butoxycarbonyl)methylene-bridged C_{60} ester when purifying the crude product using flash column chromatography, was hydrolyzed in a similar way as for C_{60}CH(COOH). The FT-IR (KBr) characterization of bisadducts shows 3427 (s), 2933 (m), 2863 (w), 1719 (s), 1640 (m), 1424 (m), 1378 (w), 1190 (s), 1035 (w), 524 (s). The compound contains a part of COO^- (1640 cm^{-1}, asymmetrical stretch). Positive APPI-MS: 837 (100, $[M - H]^+$).

Preparation of THF Solutions of Fullerene Carboxylic Acids. The MFCA and BFCA solid compounds were directly dissolved in highly pure grade and dried THF at 1.0 mg/mL with a continuous ultrasonication to form a dark-red mother solution. The stock solution was further diluted with THF to desired concentrations for other physical characterizations.

Preparation of Aqueous Solutions of Sodium Carboxylated Fullerenes. Aqueous solutions of sodium salts of the monoadducts and bisadducts were prepared following previously reported procedures:[11,21,28,34−35] 5 mL of initially made MFCA or BFCA dark red-mother solution in THF at 1.0 mg/mL was added into 50 mL of sodium hydroxide (NaOH) solution at pH = 9.5, followed by evaporation of THF at 60 °C and 350 mmHg until about 10% of its volume was evaporated off. After resetting the volume to about 50 mL with the same NaOH solution, the solution was sonicated for 1 h at 40 °C. The procedure was repeated four times, and the solvent was evaporated under reduced pressure to quantitatively remove traces of THF. The final solution was diluted to 100 mL with dilute NaOH solution in a volumetric flask to adjust the pH to 9.5. The purpose of this pH selection at 9.5 is to maximize the degree of ionization (α), which is based on the pH titration curves of fullerene hexamalonic acid and other weak acids ($\alpha = 1$ at pH = 9.5).[29]

Fourier Transform Infrared (FT-IR) Spectroscopy. The freshly made aqueous solutions of the monoadducts of sodium carboxylated fullerenes (**MSCF**) and the bisadducts of sodium carboxylated fullerenes (**BSCF**) with pH = 9.5 were mixed with IR-grade KBr, dried in a vacuum oven, and ground up, and the pellets were pressed for IR measurements. The IR spectra were collected using a Fourier transform spectrometer (Nicolet Magna 550) operating at a 2 cm^{-1} resolution.

Laser Light Scattering (LLS) Measurements. A standard LLS spectrometer (BI-200SM) equipped with a BI-9000 AT digital time correlator (Brookhaven Instrument Inc.) was used to perform LLS studies over a scattering angular range of θ = 20−150°. The temperature was controlled at 25 ± 0.1 °C. For MFCA and BFCA solutions in THF, freshly made dark-red stock solution was diluted to 0.025 mg/mL. A He−Ne laser (35 mW, 633 nm) was used to perform LLS measurements for the light-yellow solutions. For the MSCF and BSCF aqueous solutions, freshly prepared MSCF- and BSCF-stock aqueous solutions were further diluted to desired concentrations with a sodium hydroxide solution of pH = 9.5. All the solutions are colorless at the very dilute regime. A solid-state laser (DPSS, SUWTECH, 200 mW, 532 nm) was used to perform the LLS measurements. All solutions were passed through a 0.45 μm Millipore Millex-HN filter to remove dust before LLS measurements. In dynamic LLS, the Laplace inversion of each measured intensity−intensity time correlated function in a dilute solution can result in a characteristic line width distribution $G(\Gamma)$. For a purely diffusive relaxation, Γ is related to the translational diffusion coefficient D by $(\Gamma/q^2)_{C\rightarrow 0,q\rightarrow 0} = D$, where $q = (4\pi n/\lambda)\sin(\theta/2)$ with n, λ, and θ being the solvent refractive index, the wavelength of the incident light in vacuo, and the scattering angle, respectively. $G(\Gamma)$ can be further converted to a hydrodynamic radius (R_h) distribution by using the Stokes−Einstein equation, $R_h = (k_B T/6\pi\eta)D^{-1}$, where T, k_B, and η are the absolute temperature, the Boltzmann constant, and the solvent viscosity, respectively.[36] In static LLS, the angular (or q^2) dependence of net scattered intensity (I) from the self-assembled particles of fullerene surfactants is measured in a very dilute concentration (2.5×10^{-3} mg/mL). The radius of gyration $\langle R_g \rangle$ can be obtained from the linear relationship of $1/[I(q)] = C(1 + \langle R_g \rangle^2 q^2/3)$, where C is the intercept and the slope is $C\langle R_g \rangle^2/3$.

Transmission Electron Microscopy (TEM) All TEM micrographs were taken with a PHILIPS CM100 operating at an accelerating voltage of 80 kV. The samples for TEM were prepared by dropping multiple drops of solutions used in LLS measurements on copper grids with carbon or Formvar film support and waiting until the solution dried before applying the next drop. The samples were finally air dried.

Results and Discussion

Self-Association of MFCA and BFCA in THF. Since the aqueous solutions of charged MSCF and BSCF were, correspondingly, made from their acidic precursor MFCA and BFCA mother solutions in THF, it is important to examine whether certain structured aggregates were already formed from MFCA and BFCA acidic precursors in THF before they were transferred into the aqueous solution.

Figure 1 shows the apparent R_h distributions of MFCA (top) and BFCA (bottom) solutions in THF at a concentration of 2.5×10^{-5} g/mL and at two different scattering angles. Clearly, the fullerene carboxylic acids are not dissolved at the monomeric level. Both MFCA and BFCA tend to self-associate together in THF. However, the self-aggregated particles from MFCA molecules have a larger size and narrower size distributions in comparison with the aggregates from BFCA molecules. To further examine the size and morphology of MFCA and BFCA aggregates in THF, TEM images were collected from their dried solutions deposited on carbon film. As shown in Figure 2, the TEM results are consistent with the DLS results. Relative to the aggregates of BFCA molecules, the aggregates of MFCA have a larger size and are more uniformly distributed in both size and shape. The size scale of 150−250 nm of the dried MFCA aggregates and 50−150 nm of the dried BFCA aggregates in TEM images are somewhat smaller than their corresponding Z-average hydrodynamic diameters of 290 nm for MFCA aggregates and 160 nm for BFCA aggregates. This is understandable because large-sized particles contribute a much stronger scattering intensity than small particles do. The smaller size of BFCA aggregates relative to that of MFCA aggregates could be attributed to the better solubility of BFCA than that of MFCA in THF due to the additional polar carboxylic acid group per C_{60} cage. The self-association of MFCA and BFCA molecules in THF is also supported by their UV−vis spectra (see Figure 1 of Supporting Information). With the same

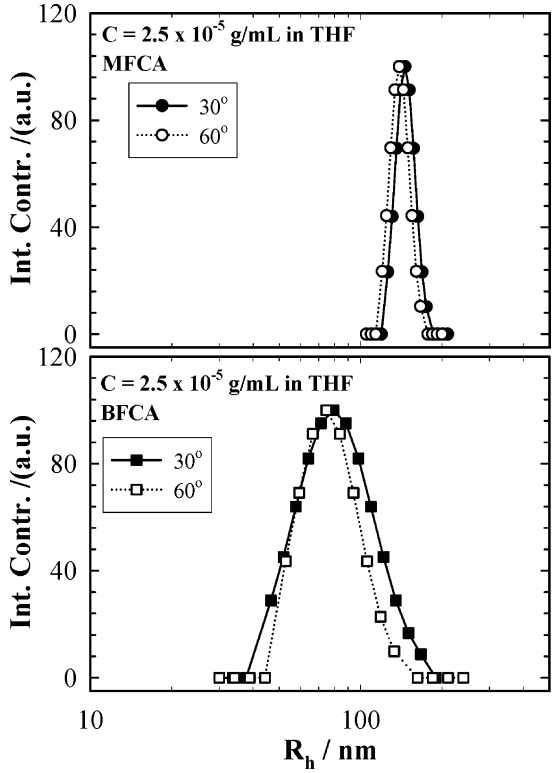

Figure 1. Apparent R_h distributions of the self-aggregates from MFCA and BFCA molecules in THF at $C = 2.5 \times 10^{-5}$ g/mL and two scattering angles of 30° and 60°.

concentration of 2.5×10^{-5} g/mL in THF, both the MFCA and BFCA solutions show a maximum at 255 nm. However, no typical peak at ~430 nm for the monomeric form of monofunctionalized fullerenes was observed,[11] suggesting that the MFCA and BFCA molecules are not at the monomeric level in THF. Relatively, the self-assembled BFCA molecules show stronger absorption than the self-assembled MFCA molecules at the higher wavelength range (i.e., 290−450 nm). This result may imply that the BFCA aggregates have stronger interactions with THF than the MFCA aggregates due to the additional polar carboxylic acid group.

Conversion of Acid to Sodium Salt of Carboxylated Fullerenes. Although the pH of the MSCF and BSCF solutions has been fixed at 9.5, not all of the acids were converted to the charged sodium carboxylate salt format. Figure 3 shows the FT-IR spectra of the freshly made MSCF (a) and BSCF (b) aqueous solutions. Obviously, the strong band located at 1566 cm^{-1} represents the sodium carboxylate (COO^-) attached on the C_{60} cage, while the very small shoulder around 1723 cm^{-1} indicates that there are still small amounts of fullerene carboxylic acids present in the MSFC and BSFC aqueous solutions. This result is consistent with the conversion of monoadducts of fullerene malonic acid $C_{60}C(COOH)_2$ to their corresponding disodium salt, in which a small amount of acid was present after neutralization with equimolar amounts of 1 M NaOH.[28] Since fullerenes could form aggregates very rapidly,[37] it is possible that the self-assembling of ionized MSCF or BSCF occurred at the same time as the MFCA or BFCA aggregates formed in THF were ionizing and reorganizing after being transferred into dilute NaOH solution. In such a case, a small fraction of fullerene carboxylic acid molecules could be encapsulated into the newly formed nanoaggregates. To support the self-assembly of the MSCF and BSCF molecules in water, the UV−vis spectra of the MSCF and BSCF aqueous solutions are provided (See Figure 2 of Supporting Information). The broad and weak

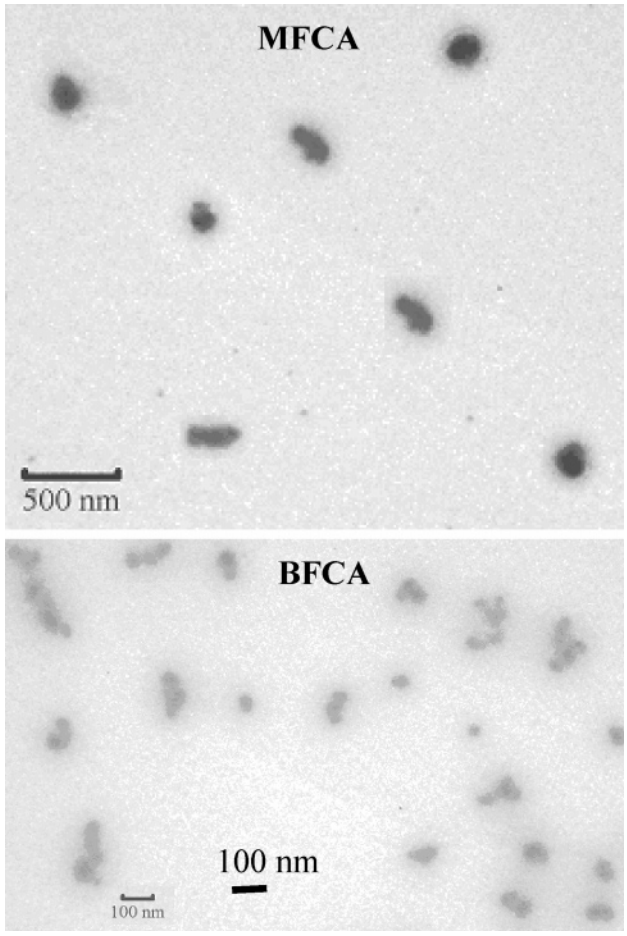

Figure 2. Typical TEM pictures of MFCA and BFCA self-aggregates formed in THF.

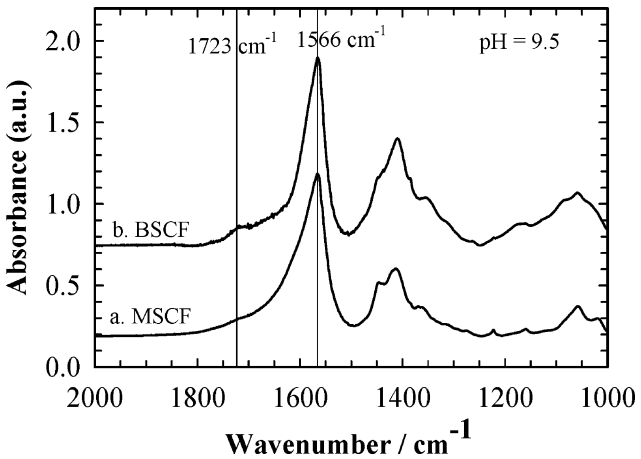

Figure 3. FT-IR spectra of the MSCF and BSCF aqueous solution at pH = 9.5.

absorption bands can be ascribed to the formation of colloidal clusters.[11,28] With a fixed concentration, the self-assembled BSCF molecules always show stronger absorption in comparison with the self-assembled MSCF molecules at the relatively higher wavelength range (i.e., >200 nm), which may imply that the self-assembled BSCF molecules have stronger interactions with water than the self-assembled MSCF molecules.

Self-Assembly of MSCF in Water. Figure 4a shows the apparent R_h distributions measured from the MSCF aqueous solution at $C = 2.5 \times 10^{-6}$ g/mL and pH = 9.5 in the scattering angle range of 20−150°. A single narrowly distributed species with an average $\langle R_h \rangle$ of about 32.5 nm was obtained. No angular

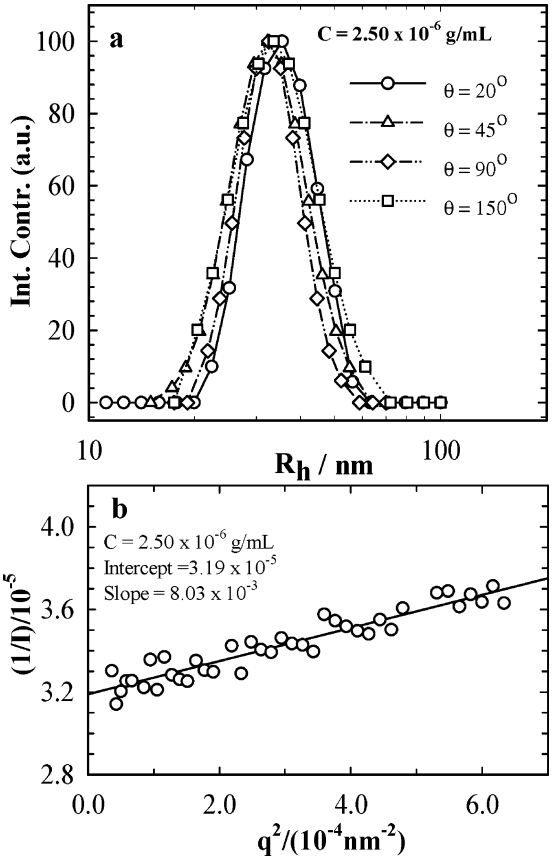

Figure 4. (a) Apparent R_h distributions of the self-assembled particles from MSCF surfactant aqueous solutions at pH = 9.5, $C = 2.5 \times 10^{-6}$ g/mL, and different scattering angles; (b) static LLS plot of the $1/[I(q)]$ versus q^2 measured from the same solution as used in (a) in the θ range of 20−100°, where $I(q)$ is the net scattered intensity from the self-assembled species in MSCF solution at different angles.

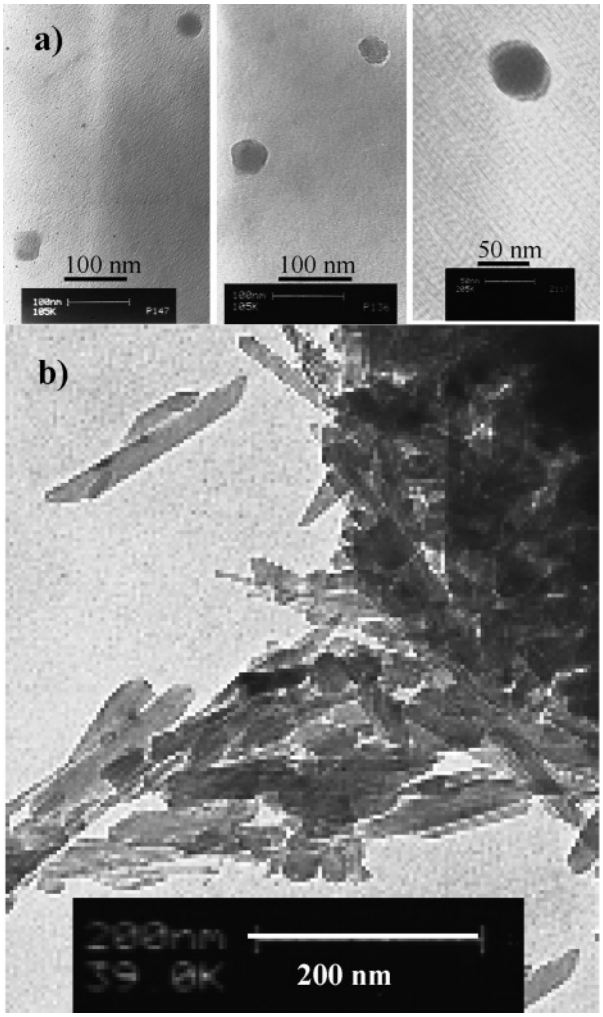

Figure 5. Typical TEM pictures of self-assembled particles from MSCF surfactants: (a) prepared from very dilute MSCF solution of 5.0×10^{-6} g/mol; (b) prepared from condensed MSCF solution of ~1 $\times 10^{-4}$ g/mL.

dependence of R_h distributions was observed within the experimental error, implying that the self-assembled particles may have a spherical conformation. To determine the morphology of the self-assembled particles from MSCF solution, static LLS was used to measure the average radius of gyration $\langle R_g \rangle$. Figure 4b shows the linear plot of the $1/[I(q)]$ versus q^2 obtained from the same MSCF aqueous solution at $C = 2.5 \times 10^{-6}$ g/mL and $\theta = 20-100°$. The linear extrapolation produces a $\langle R_g \rangle$ value of 27 ± 2 nm, which results in a ratio of $\langle R_g \rangle / \langle R_h \rangle_0 \approx 0.83$. This $\langle R_g \rangle / \langle R_h \rangle$ value is slightly larger than the value (0.774) for a hard sphere model with uniform density, indicating that the self-assembled particles from MSCF molecules have a conformation close to a hard spherical model with uniform density. This result is different from the large aggregates with $\langle R_h \rangle \approx$ 145 nm produced from MFCA molecules in THF, which confirms that the initially formed MFCA aggregates in THF are dissolved and reorganized after being transferred into NaOH solution.

Figure 5a shows a few representative TEM images made from the dilute MSCF solution of 5.0×10^{-6} g/mL, which clearly supports our LLS results that the self-assembly of MSCF surfactants produces solid and spherical particles with nearly uniform density. The dried spherical particles have a typical size range from 40 to 60 nm in diameter, which is reasonable in comparison with the *Z*-average hydrodynamic diameter of ~65 nm from dynamic LLS. Since the TEM samples were prepared from the very dilute MSCF aqueous solution, the number density of self-assembled spherical particles on the copper grid is low, and only individual spheres were observed. When the dilute MSCF aqueous solution was condensed to higher concentration via rotative evaporation of water under reduced pressure, the solid spheres tend to aggregate together to form irregularly shaped and rodlike solid aggregates as shown in Figure 5b. The strong tendency of interparticle association at higher concentrations could also be reflected from the concentration dependence of the apparent diffusion coefficient D_{app} measured at a scattering angle $\theta = 30°$ (see Figure 3 of Support Information), which shows a negative diffusion second virial coefficient. In other words, the apparent R_h increases with an increase in concentration.

Self-Assembly of BSCF in Water. Figure 6a shows the apparent R_h distributions measured from the BSCF aqueous solution at $C = 1.68 \times 10^{-6}$ g/mL and pH = 9.5 in the scattering angle range of 30−90°. Different from the single-mode distributions of the dilute MSCF aqueous solutions, bimodal distributions are observed. While the small species with a $\langle R_h \rangle$ of 23 nm shows no angular dependence in size, the intensity contribution from the small species gradually increases as the scattering angle is increased. For the large species, their size has apparent angular dependence, implying a nonglobular conformation. Although the small species contributed a very small fraction to total scattered intensity at low scattering angle, the concentration of the small species is approximately twice as high as that of the large species in the BSCF solutions based on the relationship

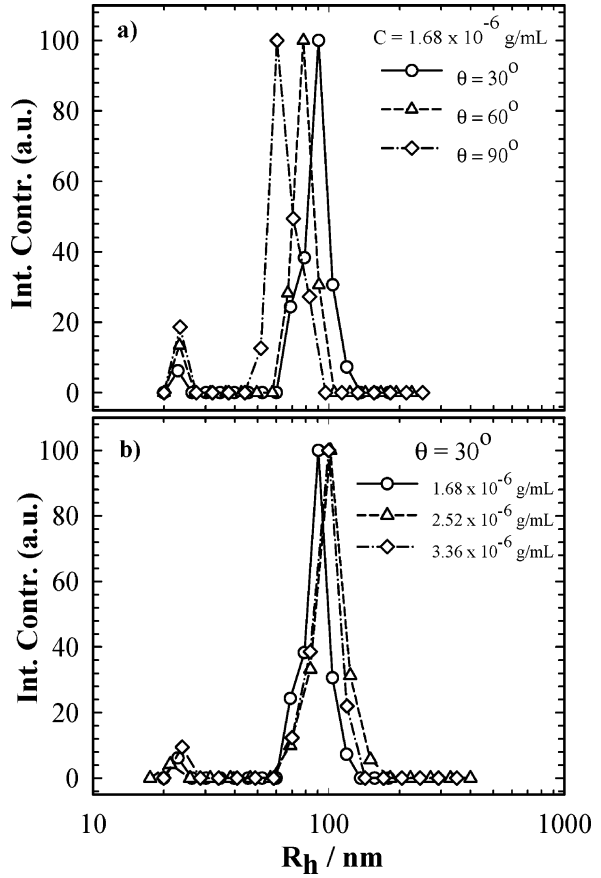

Figure 6. Apparent R_h distributions of the self-assembled particles from BSCF surfactant aqueous solutions at pH = 9.5. (a) $C = 1.68 \times 10^{-6}$ g/mL and $\theta = 30-90°$; (b) $\theta = 30°$, and $C = 1.68 \times 10^{-6} - 3.36 \times 10^{-6}$ g/mL.

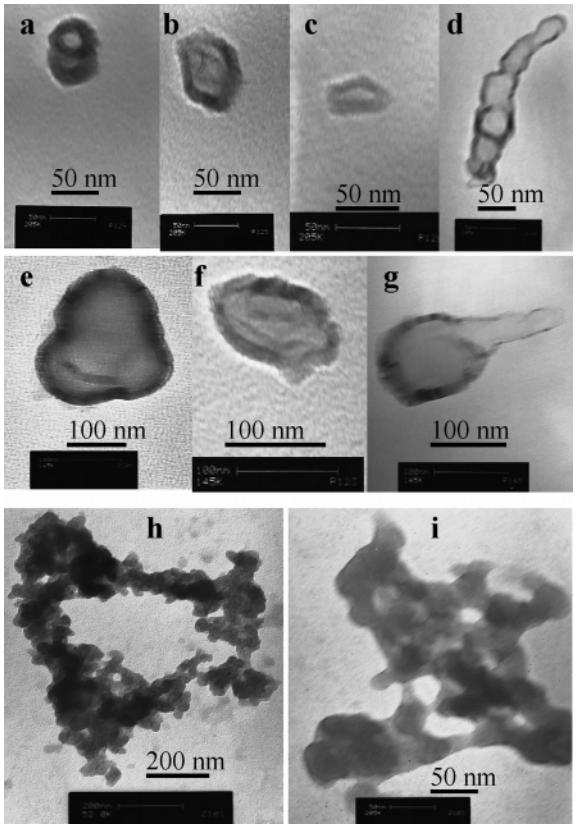

Figure 7. Typical TEM pictures of self-assembled hollow shells from BSCF surfactants: (a−g) prepared from very dilute BSCF solution of 2.1×10^{-5} g/mL; (h, i) prepared from condensed BSCF solution of $\sim 2.5 \times 10^{-4}$ g/mL.

of $I \propto C\langle R_h\rangle^3$. The extrapolation of the apparent $\langle R_h\rangle$ measured at different angles to the zero angle produces a $\langle R_h\rangle_0$ of 104 nm for the large species. It should be mentioned that the particles formed in BSCF aqueous solutions are very stable. No change was observed in terms of R_h distributions after the dilute BSCF solutions were set for two months. Moreover, as shown in Figure 6b, the size of the self-assembled particles from BSCF does not show apparent concentration dependence in the dilute regime from 1.68×10^{-6} to 3.36×10^{-6} g/mL. The distinct bimodal distributions of BSCF aggregates in aqueous solution with $\langle R_h\rangle \approx 23$ nm and ≈ 104 nm, which are different from the polydispersed single-mode distributions of $\langle R_h\rangle \approx 160$ nm from BFCA aggregates in THF, indicating that the initially formed BFCA aggregates in THF were at least partially dissolved after being transferred into dilute NaOH solution due to the ionization. A question arises now whether the ionized BSCF molecules reorganize into new structures in aqueous solutions.

To examine the size and morphologies of the self-assembled particles from BSCF molecules in water, TEM pictures were taped from the samples made from the dilute BSCF aqueous solution. Figure 7a−g shows some representative TEM images with a few important features. *First*, no solid particles were observed. Instead, only the morphology of hollow shells appeared although the shape and size vary. These hollow-shell structures are apparently different from the irregular aggregates formed from the acidic BFCA molecules in THF, which indicates that the initial BFCA aggregates formed in THF do dissolve and reorganize after being transferred into NaOH aqueous solution. *Second*, there are two major species in terms of the size of the hollow shells. The small species are mainly in distorted spherical shapes, having average diameters of about 50−60 nm (a−c), while the large fullerene aggregates can be either the distorted hollow spheres with long axial dimension in the range of 140−220 nm (e−g) or in a very extended tube shape joined by five small hollow shells with a total tube length of ∼270 nm and a tube diameter of 45−55 nm (d). Considering the possible collapse of the hollow shells during the drying process for TEM sample preparation, the two major size ranges observed from TEM graphs are basically consistent with the dynamic LLS results. The irregularly distorted nonspherical shapes of the large hollow shells observed in TEM explain the apparent angular dependence of the R_h distributions for the large species observed in dynamic LLS. *Third*, the number density of the self-assembled hollow shells is low, and in most cases, only individual hollow shells were observed due to the very dilute BSCF concentration applied for TEM sample preparation. There are two possible reasons to explain the partial overlap of two small hollow shells in picture (a) and the long tube from the connection of five small hollow shells in picture (d). One is the physical overlap of hollow shells related to our TEM sample preparation procedure in which we applied the very dilute solutions drop by drop to the copper grid and waited until the solution dried before applying the next drop. Another is that there may still exist some interparticle association even at very dilute concentration. In fact, the interparticle association can be dramatically increased when the dilute BSCF solution was condensed to higher concentration via rotative evaporation of water under reduced pressure. As shown in Figure 7(h,i), the hollow shells tend to associate and melt together to form a three-dimensional network at high concentrations.

The size and shape difference of the self-assembled hollow shells from BSCF molecules in dilute aqueous solutions might

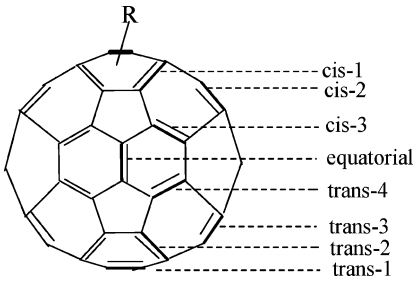

Figure 8. Positional relationships of the eight different double bonds in a C_{60} monoadduct relative to the 6−6 bond carrying the first addent R.

be attributed to the variety of the relative positions of the two charged carboxyl groups on the C_{60} cages. The BSCF molecules may consist of a few isomers due to regiochemistry. Hirsch et al. isolated and characterized seven isomers of bis(ethoxycarbonyl)methylene-C_{60}.[38] They found that the ratio of the bisadducts at different relative positions is 38:30:13:9:6:2:2 at equatorial, *trans*-3, *trans*-2, *trans*-4, *cis*-3, *cis*-2, and *trans*-1, respectively, relative to the addent already bound to the fullerene core (see Figure 8), indicating that the most favorable relative positions are at the equatorial and *trans*-3 positions. Considering the same synthetic mechanisms for the ester precursors of our bisadducts of fullerene carboxylic acid, the BSCF molecules should have a similar isomer ratio, namely, two isomers will be the dominant species. One has a relative position of the two charged carboxyl groups on the C_{60} cage separated by about 90° (equatorial), another has the two charged carboxyl groups distant by about 135° (*trans*-3). This relative position difference of the two charges on the rigid C_{60} surface can generate different hydrophilic/hydrophobic interfacial geometry. We speculate that the different hydrophilic/hydrophobic interfacial geometry from the two dominant isomers might be related to the two major size ranges of hollow shells being determined from LLS and TEM measurements. The presence of other minor isomers might provide a variety of local interfacial geometries, leading to different distortions of the spherical vesicles into various shapes of hollow shells. Nevertheless, our results that BSCF molecules self-assemble to form hollow shells and MSCF molecules self-associate to form solid spherical particles in aqueous solutions indicate that the number of charged appendages on the fullerene cage could be one important molecular structural property to control the morphology of fullerene aggregates. The size of the hydrophilic carboxyl group is much smaller than the ball-like hydrophobic C_{60} cage. For MSCF molecules, only one carboxylate group is attached on the C_{60} cage. For BSCF molecules, two carboxylate groups are attached on the C_{60} cage and are separated by about 90° (equatorial) and 135° (*trans*-3). To make sure the carboxyl groups are sticking out into the water phase, the hydrophilic/hydrophobic interface of BSCF molecules would be more flat than that of MSCF molecules. The flatter hydrophilic/hydrophobic interface might lead to a vesicle structure, as a zero hydrophilic/hydrophobic interfacial curvature produces lamellar packing.[39]

Conclusions

Both monoadducts and bisadducts of fullerene carboxylic acids are soluble in THF but not in the monomeric state. They tend to self-associate together to form large particles. The size of the aggregates from bisadducts is smaller than that of the aggregates from monoadducts due to the better solubility of bisadducts in THF. After being transferred into dilute NaOH aqueous solution, these fullerene carboxylic acid aggregates dissolved and reorganized with the ionization of carboxylic acid groups. The self-assembly of the monoadducts of sodium carboxylate fullerenes results in small, solid spherical particles with a nearly uniform density. In contrast, the self-assembly of bisadducts of sodium carboxylate fullerenes only generates hollow shells in water. The condensation of the dilute, solid spherical particle solutions from monoadducts produces rodlike and irregularly shaped large aggregates, while the condensation of the dilute vesicle solutions from bisadducts generates three-dimensional networks. The vesicle formation of BSCF molecules in water instead of the solid particles formed in the MSCF aqueous solution might be attributed to the flatter hydrophilic/hydrophobic interface of BSCF molecules.

Acknowledgment. S.Z. acknowledges the financial support of this work from the National Science Foundation (CHE 0316078). We thank Professor William L'Amoreaux (Department of Biology at CSI) for continuous help with TEM experiments.

Supporting Information Available: UV−visible spectra of the self-aggregated MFCA and BFCA molecules in THF and the self-assembled MSCF and BSCF molecules in water as well as the concentration dependence of the apparent diffusion coefficient of the self-assembled MSCF molecules. This material is available free of charge via the Internet at http://pubs.acs.org.

References and Notes

(1) Dresselhaus, M. S.; Dresselhaus, G.; Eklund, P. C. *Science of Fullerenes and Carbon Nanotubes*, Academic Press: San Diego, CA, 1996.
(2) Echegoyen, L.; Echegoyen, L. E. *Acc. Chem. Res.* **1998**, *31*, 593.
(3) Guldi, D. M.; Prato, M. *Acc. Chem. Res.* **2000**, *33*, 695.
(4) Martin, N.; Sanchez, L.; Illescas, B.; Perez, I. *Chem. Rev.* **1998**, *98*, 2527.
(5) Schon, J. H.; Kloc, C. H.; Batlogg, B. *Science* **2001**, *293*, 2432.
(6) Schuster, D. I.; Wilson, S. R.; Schinazi, R. F. *Bioorg. Med. Chem. Lett.* **1996**, *6*, 1253.
(7) Wilson, S. R. Nanomedicine: Fullerene and Carbon Nanotube Biology. In *Perspectives of Fullerene Nanotechnology*; Osawa, E., Ed.; Kluwer Academic: Dordrecht, 2002; pp 155−163.
(8) Nakamura, E.; Isobe, H. *Acc. Chem. Res.* **2003**, *36*, 807.
(9) Innocenzi, P.; Brusatin, G. *Chem. Mater.* **2001**, *13*, 3126.
(10) Da Ros, T.; Prato, M.; Novello, F.; Maggini, M.; Banfi, E. *J. Org. Chem.* **1996**, *61*, 9070.
(11) Angelini, G.; Maria, P. D.; Fontana, A.; Pierini, M.; Maggini, M.; Gasparrini, F.; Zappia, G. *Langmuir* **2001**, *17*, 6404.
(12) Kordatos, K.; Ros, T. D.; Bosi, S.; Vazquez, E.; Bergamin, M.; Cusan, C.; Pellarini, F.; Tomberli, V.; Baiti, B.; Pantarotto, D.; Georgakilas, V.; Spalluto, G.; Prato, M. *J. Org. Chem.* **2001**, *66*, 4915.
(13) Pantarotto, D.; Bianco, A.; Pellarini, F.; Tossi, A.; Giangaspero, A.; Zelezetsky, I.; Briand, J.; Prato, M. *J. Am. Chem. Soc.* **2002**, *124*, 12543.
(14) Prato, M.; Maggini, M. *Acc. Chem. Res.* **1998**, *31*, 519.
(15) Richardson, C. F.; Schuster, D. I.; Wilson, S. R. *Org. Lett.* **2000**, *2*, 1011.
(16) Sawamura, M.; Kawai, K.; Matsuo, Y.; Kanie, K.; Kato, T.; Nakamura, E. *Nature* **2002**, *419*, 702.
(17) Shi, Z.; Li, Y.; Wang, S.; Du, C.; Xiao, S.; Fang, H.; Zhou, Y.; Zhu, D. *Solid State Commun.* **2001**, *120*, 269.
(18) Taton, D.; Angot, S.; Gnanou, Y.; Wolert, E.; Setz, S.; Duran, R. *Macromolecules* **1998**, *31*, 6030.
(19) Isobe, H.; Mashima, H.; Yorimitsu, H.; Nakamura, E. *Org. Lett.* **2003**, *5*, 4461.
(20) Cassell, A. M.; Asplund, C. L.; Tour, J. M. *Angew. Chem., Int. Ed.* **1999**, *38*, 2403.
(21) Zhou, S.; Burger, C.; Chu, B.; Sawamura, M.; Nagahama, N.; Toganoh, M.; Hackler, U. E.; Isobe, H.; Nakamura, E. *Science* **2001**, *291*, 1944.
(22) Sano, M.; Oishi, K.; Ishi-I, T.; Shinkai, S. *Langmuir* **2000**, *16*, 3773.
(23) Verma, S.; Hauck, T.; El-Khouly, M. E.; Padmawar, P. A.; Canteenwala, T.; Pritzker, K.; Ito, O.; Chiang, L. Y. *Langmuir* **2005**, *21*, 3267.
(24) Nakashima, N.; Ishii, T.; Shirakusa, M.; Hiroto, T.; Sagara, M. *Chem.−Eur. J.* **2001**, *7*, 1766.
(25) Song, T.; Dai, S.; Tam, K. C.; Lee, S. Y.; Goh, S. H. *Langmuir* **2003**, *19*, 4798.

(26) Georgakilas, V.; Pellarini, F.; Prato, M.; Guldi, D. M.; Melle-Franco, M.; Zerbetto, F. *Proc. Natl. Acad. Sci. U.S.A.* **2002**, *99*, 5075.
(27) Guldi, D. M.; Zerbetto, F.; Georgakilas, V.; Prato, M. *Acc. Chem. Res*. **2005**, *38*, 38.
(28) Guldi, D. M.; Hungerbuhler, H.; Asmus, K. D. *J. Phys. Chem.* **1995**, *99*, 13487.
(29) Cerar, J.; Cerkovnik, J.; Skerjanc, J. *J. Phys. Chem. B* **1998**, *102*, 7377.
(30) Cerar, J.; Skerjanc, J. *J. Phys. Chem. B* **2000**, *104*, 727.
(31) Cerar, J.; Skerjanc, J. *J. Phys. Chem. B* **2003**, *107*, 8255.
(32) Issacs, L.; Wehrsig, W.; Diederich, F. *Helv. Chim. Acta* **1993**, *76*, 1231.
(33) Issacs, L.; Diederich, F. *Helv. Chim. Acta* **1993**, *76*, 2454.
(34) Sawamura, M.; Nagahama, N.; Toganoh, M.; Hackler, U. E.; Isobe, H.; Nakamura, E.; Zhou, S.; Chu, B. *Chem. Lett.* **2000**, *9*, 1098.
(35) Deguchi, S.; Alargova, R. G.; Tsuji, K. *Langmuir* **2001**, *17*, 6013.
(36) Chu, B. *Laser Light Scattering*, 2nd ed.; Academic Press: New York, 1991.
(37) Alargova, R. G.; Deguchi, S.; Tsujii K. *J. Am. Chem. Soc.* **2001**, *123*, 10460.
(38) Hirsch, A.; Lamparth, I.; Karfunkel, H. R. *Angew. Chem., Int. Ed. Engl.* **1994**, *33*, 437.
(39) Lindblom, G.; Rilfors, L. *Biochim. Biophys. Acta* **1989**, *988*, 221.